European Journal of Soil Science

WILEY

RESEARCH ARTICLE OPEN ACCESS

Organic Carbon and Texture Control Moisture Dependence of Soil Shortwave Infrared Reflectance

D. Hick[1] | P. J. Chapman[1] | T. S. Breure[2] | G. Ziv[1]

[1]School of Geography, University of Leeds, Leeds, UK | [2]European Commission, Joint Research Centre, Ispra, Italy

Correspondence: D. Hick (eedh@leeds.ac.uk)

Received: 17 June 2025 | **Revised:** 10 December 2025 | **Accepted:** 23 March 2026

Keywords: cropland | Europe | LUCAS | soil moisture | soil properties | soil spectroscopy | soil type

ABSTRACT

Moisture content affects soil reflectance in the optical domain (400–2500 nm), acting as a confounding factor in soil property prediction models. Soil reflectance needs to be simulated efficiently for varying levels of soil moisture, in order to aid soil property prediction efforts and inform physical land surface models. Here, we built on previous work that investigated how soil reflectance decreases with increasing soil moisture. We explored how the relationship between the reflectance and soil moisture content changes as a function of wavelength and soil characteristics. For this purpose, we acquired the spectra of 28 soil samples from various locations across Europe in a laboratory setting, at different levels of soil moisture. The soil reflectance-moisture relationship was found to be wavelength-dependent and best represented by decreasing exponential functions. The rates of exponential decrease, however, varied across soil samples and were normalised to isolate effects of different soil characteristics. It was found that organic carbon (OC), clay and silt content displayed a statistically significant relationship with the normalisation factor, a proxy for how quickly soil 'darkens' with increasing soil moisture content. A multiple linear regression model was used to describe the normalisation factor based on OC content and soil textural information. The resulting model was able to explain 67% of the variance, with OC and clay content accounting for almost 70% of the relative feature importance. Our findings call for the inclusion of OC content and textural information, especially clay content, in physical models of soil moisture-reflectance, for more efficient simulations of soil reflectance at varying levels of soil moisture, to support climate models and soil property predictions efforts based on field and remotely sensed data.

1 | Introduction

Soil reflectance, defined as the ratio of incident to reflected light intensity across different wavelengths, is influenced by the chemical, physical, and biological characteristics of soil (Li et al. 2021). In the visible (VIS) range of the electromagnetic spectrum (400–700 nm), soil reflectance is affected by iron oxide content, which confers a red-brown or yellow hue to the soil and is contained in minerals such as hematite and goethite, respectively (Ben-Dor and Demattê 2015). In the near-infrared and shortwave infrared (NIR-SWIR, 700–2500 nm), reflectance is affected by the OH group of clay minerals and the C—O bond of carbonates (Ben-Dor and Demattê 2015). Organic carbon (OC) content has a pervasive effect on reflectance across the entire optical domain, as does soil texture, because coarser particles result in an irregular surface that can cause micro-shadowing effects (see Baumgardner et al. 1986).

Soil reflectance provides a fingerprint of soil properties and can be used to calibrate soil spectra against traditional laboratory measurements to obtain quantitative estimates, a technique known as soil spectroscopy (Viscarra Rossel et al. 2022). In soil spectroscopy studies, soil samples are typically air or oven-dried and finely milled in a laboratory to avoid the confounding effects of soil moisture content and variable particle size (Nocita et al. 2015). However, in real-world settings, soil moisture

Highlights

- Reflectance-moisture relationship of 28 European soils varies based on wavelength and soil type.
- Rate of reflectance decrease with increasing moisture was normalised across different soil types.
- OC, clay, and silt content affected the rate of reflectance decrease with increasing soil moisture.
- Model proposed to describe soil reflectance decrease with moisture based on soil OC and texture.

content is rarely zero, and is highly spatially and temporally variable (Ben-Dor and Demattê 2015; Castaldi et al. 2015).

Water can be found in the soil matrix in three separate forms: incorporated into the mineral lattice (hydrated), adsorbed bound to the surface of the soil particles as a thin layer (hygroscopic), or as free water occupying the pore space (which makes up ~50% of soil volume), to varying degrees until saturation, when all pore space is filled by water (Ben-Dor 2002). While hygroscopic water causes OH absorption features around 1400 and 1900 nm, free water decreases soil reflectance across the whole electromagnetic spectrum (Ben-Dor and Demattê 2015). In fact, to the human eye, soil looks darker when wet, which was first investigated in the laboratory around 100 years ago (Ångström 1925). This phenomenon has been attributed to the refractive index of soil being more similar to that of water than that of air, which results in decreased light scattering when soil moisture content increases, leading to decreased soil reflectance (Twomey et al. 1986). It is now widely accepted that the SWIR region (1000–2500 nm) is particularly suited to monitor changes in soil moisture, because reflectance in this region continues to respond to increasing volumetric soil water content (until ~50%), whereas visible wavelengths saturate at around 20% (Lobell and Asner 2002). More recently, physical models have been developed that rely on the principles of radiative transfer theory, such as MARMIT and MARMIT-2, which represent wet soil as a layer of dry soil covered by a layer of water (Bablet et al. 2018; Dupiau et al. 2022). The downsides of physical models like MARMIT, however, are that input parameters are difficult to determine and soil properties are not accounted for (Sadeghi et al. 2015).

Satellite soil reflectance can be used to derive soil albedo, an important input to climate and land surface models. Nevertheless, in these models, the variation in soil albedo due to surface soil moisture is either ignored or oversimplified (He et al. 2019; Liu et al. 2014). The relationship between soil albedo, soil moisture and soil properties is still poorly understood and could introduce uncertainty in climate models (He et al. 2019). Furthermore, moisture in field or remotely-sensed spectra can affect and mask the reflectance signals of other soil properties, consequently skewing spectroscopy-based soil property predictions (Knadel et al. 2023). With the increasing emergence of narrowband hyperspectral satellites and handheld devices for in situ soil monitoring, it is increasingly relevant to account for the presence of water in spectra acquired under field conditions (Sanderman et al. 2025). The confounding effect of soil moisture can be removed by mathematical techniques, such as external parameter orthogonalisation (EPO) (Roger et al. 2003). EPO has been shown to improve prediction of soil OC content for spectral measurements collected at variable levels of soil moisture (Minasny et al. 2011). EPO requires a large calibration dataset; however, of ideally at least 60 samples, for which soil properties and soil spectra at different levels of soil moisture need to be measured in laboratory conditions (Minasny et al. 2011).

At the same time, other semi-empirical studies based on spectroscopic observation describe soil reflectance as a function of soil moisture using, for instance, regression (Lobell and Asner 2002; Muller and Decamps 2001) or spectral soil moisture band ratio indices (Haubrock et al. 2008). It is generally accepted that soil reflectance decreases exponentially with increasing soil moisture content (Lobell and Asner 2002), and that this relationship decreases non-linearly until a critical water saturation point, determined by the soil's hydraulic properties, beyond which reflectance increases with increasing soil moisture (Weidong et al. 2002). Other studies have suggested a linear regression model best approximates this relationship (McGuirk and Cairns 2024; Muller and Decamps 2001). However, few models exist that were validated on different soil types, and the connection between soil properties, soil moisture content and spectral reflectance remains a problem to be addressed (Dupiau et al. 2022; Tian and Philpot 2015).

In this study, the laboratory soil moisture-reflectance relationship in the optical domain was investigated for 28 different European soils. Our goal was two-fold: (i) to identify which soil properties affect the soil moisture-reflectance relationship; (ii) to develop a semi-empirical model that describes how soil properties affect reflectance under varying moisture content. The results could be included in physical climate models to obtain more reliable bare soil albedo estimates based on soil moisture and soil properties, or in future simulations of soil reflectance for varying levels of soil moisture to improve soil property predictions using field or remotely sensed spectra.

2 | Methods

Across the European Union, soil properties are monitored through the Land Use/Coverage Area Frame Survey (LUCAS) soil module, a soil sampling campaign aimed at collecting harmonised soil property information at 0–20 cm depth. The most recent LUCAS survey for which data is publicly available was carried out in 2018, and a total of 18,984 samples were analysed (Fernandez-Ugalde et al. 2022).

The Joint Research Centre (JRC) in Ispra (Italy) provided subsamples for 27 topsoil samples from the LUCAS 2018 survey. We briefly describe the selection procedure of the 27 samples. First, we restricted the LUCAS 2018 database to include samples for which organic carbon (OC), $CaCO_3$ content, bulk density and oxalate iron (Ox_Fe) content were measured. Second, we excluded samples belonging to non-annual cropland (olive groves, vineyards, other fibre and oleaginous crops, tomatoes, strawberries, nurseries, floriculture and ornamental plants, other citrus fruits, other fruit trees and berries, cherry fruit, pear fruit, apple fruit, oranges, nuts trees, permanent industrial crops). Third, we restricted ourselves to the locations that were repeated across the LUCAS surveys and appended LUCAS 2009 sand, silt and clay information, with sand referring to soil particles of size 2–0.05 mm, silt to particles of size 0.05–0.002 mm and clay particles of size < 0.002 mm (Jones et al. 2020). These steps resulted in a total of 388 samples.

The cube algorithm (Grafström and Lisic 2018) was then used to select samples ($n=27$) balanced on OC, clay, $CaCO_3$, Ox_Fe content and spread across location (latitude and longitude). All covariates were scaled to unit variance. We specifically chose the cube algorithm to approximate the distributions of the target covariates, while maximising the geographical spread across Europe, to increase the variability of soil conditions within the selected sample. We then located 26 of these samples in the LUCAS soil archive and obtained subsamples from each of ~60 g. As one of the target samples selected by the cube algorithm could not be located in the LUCAS soil archive, and the LUCAS 2018 Spanish samples had not been archived at the time of soil sample selection, one sample from Spain with similar OC, clay and $CaCO_3$ content as the original sample was selected instead from the unarchived samples to improve coverage in this Mediterranean region. Finally, to extend coverage beyond the European Union, one additional sample was collected in August 2023 from the University of Leeds research farm in northern England (53° 52′ 25.2″ N, 1° 19′ 47.0″ W). Its soil properties were measured at the University of Leeds Geography laboratories following the same protocols as LUCAS when possible: dry combustion for OC content (EuroEA3106), pyrophosphate extraction and ICP analysis for Ox_Fe content (Blakemore et al. 1987), titration for $CaCO_3$ content (Allen et al. 1974) and settling, sieving and gravimetry for particle size (van Reeuwijk 1995). A map of the selected soil samples is shown in Figure 1, while a summary of the properties of the soil samples used in this study is presented in Table 1.

The 28 samples used in this study represent a proportional subset of European cropland soils. The dataset is largely composed of Luvisols and Cambisols—the dominant agricultural soil types across the EU, accounting for ~55% of LUCAS 2018 topsoil cropland points—with limited representation of Podzols and Regosols, and no representation of other soil types such as Planosols or Calcisols. Three Mediterranean soils were included. Soil hue, indicating colour variability driven by mineralogical differences (e.g., $CaCO_3$ and iron oxides), was measured using the Munsell colour chart to illustrate the chromatic range of the samples (see Table 1). Although this dataset does not capture the full pedological or chromatic diversity of European cropland soils, it includes a large proportion of the dominant soil types used for cropland across the EU (Cambisols and Luvisols), and

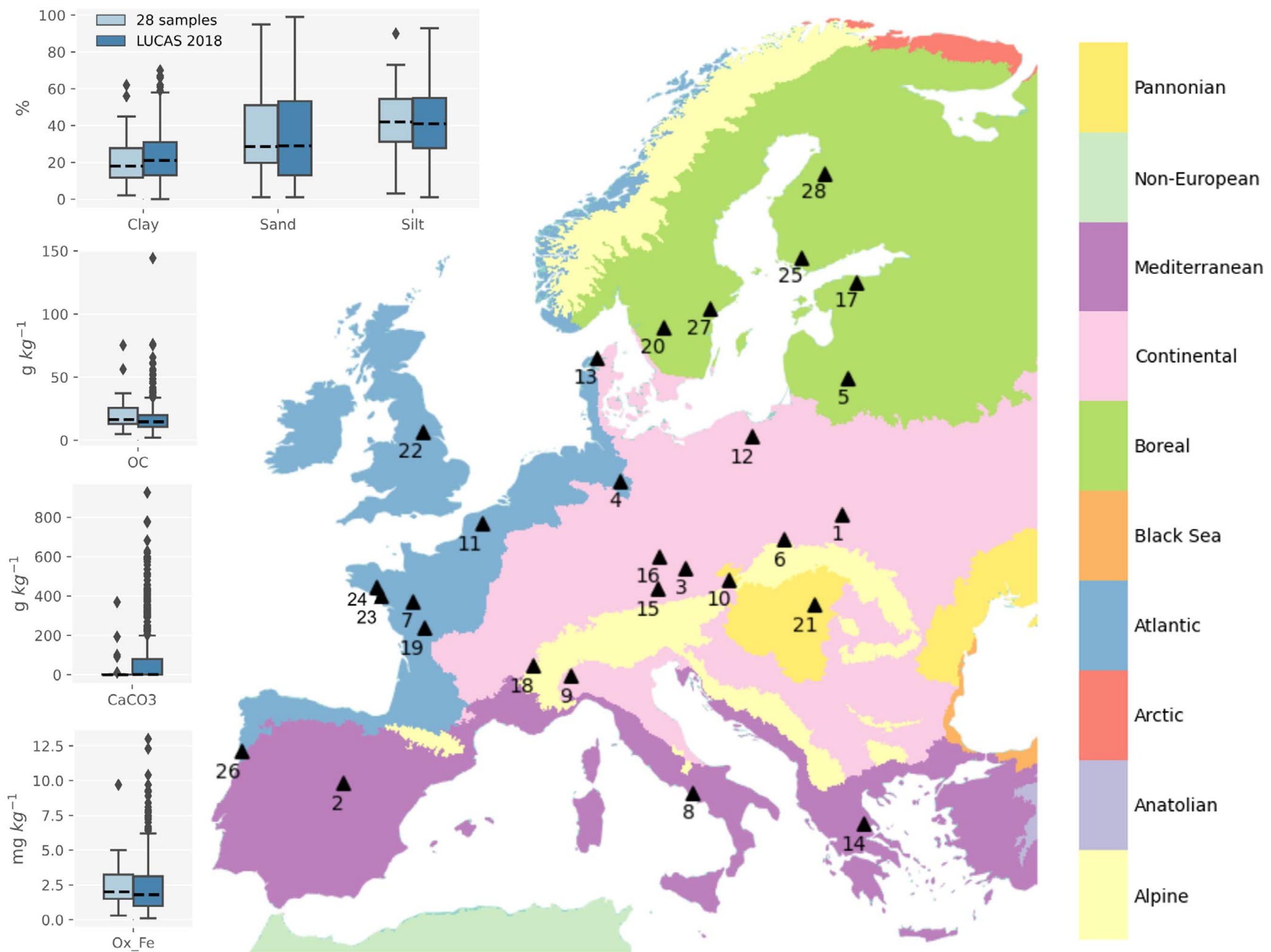

FIGURE 1 | Provenance of the 28 soil samples used in this study against European biogeographical regions and their properties in comparison to cropland LUCAS 2018 topsoil data. *Source:* EEA (2016).

TABLE 1 | Soil properties of samples (0–20 cm depth) used in this study.

ID	Country	USDA textural class	Soil type	Hue	Value	Chroma	OC ($g\,kg^{-1}$)	Clay (%)	Sand (%)	Silt (%)	$CaCO_3$ ($g\,kg^{-1}$)	Ox_Fe ($mg\,kg^{-1}$)	BD 0–20 ($g\,cm^{-3}$)
1	PL	Silt	Luvisol	10YR	5	3	5.0	8	2	90	0	1.1	1.41
2	ES	Sandy loam	Leptosol	10YR	6	4	7.6	20	44	36	2	3.6	0.95
3	CZ	Sandy loam	Luvisol	2.5Y	6	3	9.2	14	66	21	0	4.8	1.57
4	DE	Sandy loam	Gleysol	2.5Y	5	3	9.7	11	68	22	0	2.3	1.51
5	LT	Sandy loam	Luvisol	10YR	6	4	10.1	11	61	27	0	2.0	1.53
6	PL	Silt loam	Luvisol	2.5Y	6	3	10.8	17	10	73	3	3.4	1.11
7	FR	Loam	Cambisol	10YR	5	3	12.5	11	47	42	1	4.1	1.38
8	IT	Silt loam	Luvisol	10YR	5	4	13.2	13	30	56	1	0.3	0.88
9	IT	Silt loam	Anthrosol	2.5Y	5	3	13.2	20	20	59	1	1.8	1.07
10	AT	Loam	Chernozem	10YR	4	3	13.7	22	44	33	11	0.6	1.30
11	FR	Silty clay loam	Luvisol	2.5Y	6	4	14.0	31	19	49	0	3.2	1.04
12	PL	Loam	Luvisol	2.5Y	6	4	14.1	19	39	43	100	1.9	1.05
13	DK	Sand	Arenosol	10YR	5	2	15.5	2	95	3	0	0.6	1.57
14	EL	Silty clay	Fluvisol	5Y	6	2	15.9	45	4	52	369	0.7	0.81
15	DE	Silt loam	Cambisol	2.5Y	6	3	17.0	16	27	56	0	3.1	1.28
16	CZ	Silt loam	Cambisol	10YR	4	2	17.3	27	20	53	0	4.5	1.36
17	EE	Loam	Cambisol	2.5Y	6	3	18.8	15	49	37	91	1.9	1.41
18	FR	Clay loam	Leptosol	2.5Y	6	4	21.6	34	24	42	193	1.2	1.26
19	FR	Clay	Cambisol	2.5Y	6	4	22.1	41	26	33	1	4.2	1.04
20	SE	Sandy loam	Cambisol	10YR	4	2	23.3	7	63	29	0	3.2	1.09
21	HU	Silty clay loam	Arenosol	10YR	3	2	25.7	30	3	67	2	1.8	1.51
22	UK	Sandy loam	Cambisol	10YR	5	4	25.8	16	55	32	60	2.7	1.22
23	FR	Silt loam	Cambisol	2.5Y	6	4	27.9	21	26	54	0	1.6	1.31
24	FR	Silt loam	Cambisol	10YR	4	3	31.0	17	16	67	0	5.0	1.18

(Continues)

TABLE 1 | (Continued)

ID	Country	USDA textural class	Soil type	Hue	Value	Chroma	OC ($g\,kg^{-1}$)	Clay (%)	Sand (%)	Silt (%)	$CaCO_3$ ($g\,kg^{-1}$)	Ox_Fe ($mg\,kg^{-1}$)	BD 0–20 ($g\,cm^{-3}$)
25	FI	Clay	Cambisol	2.5Y	4	2	34.3	62	20	18	1	9.7	1.11
26	PT	Sandy loam	Regosol	10YR	6	3	37.3	12	57	32	0	3.2	0.99
27	SE	Silty clay	Cambisol	10YR	5	2	56.3	56	1	43	0	0.6	1.02
28	FI	Loamy sand	Podzol	10YR	4	2	75.3	4	86	9	0	2.0	1.26

it was selected specifically to represent the variation in key soil properties relevant to optical behaviour: wide ranges of OC content (5–75.3 $g\,kg^{-1}$), clay (2%–62%), sand (1%–95%), silt (3%–90%), $CaCO_3$ (0–369 $g\,kg^{-1}$) and Ox_Fe content (0.3–9.7 $mg\,kg^{-1}$) were captured in the selected samples.

On return to the University of Leeds laboratories, all soil samples were oven-dried at 30°C for 48h to remove any residual soil moisture, and sieved to 2mm. For each sample, ~50g of soil was placed into 90-mm diameter petri dishes, producing a layer approximately 0.7cm thick (see Appendix A, Figure A1). The amount of soil added to the petri dish was calculated to approximate the field bulk density measured in situ, ensuring that the soil volume and packing conditions during measurement reflected field conditions as closely as possible. Although rock fragment content was not accounted for, lightly packing the soil allowed us to reproduce the target bulk density, which can affect spectral behaviour under controlled conditions. Then, the 350–2500nm reflectance of the dry soil samples was collected in the laboratory at a sampling interval of 1nm using an SVC 1024HR-i spectroradiometer. This was fitted with a hand-held contact probe, connected via an optical fibre and containing a 5W tungsten halogen light source. The contact probe was held perpendicular to and in direct contact with the soil surface to reduce the effect of surrounding light and atmospheric water content during scans (see Appendix A, Figure A2a). We wanted to use the same protocol for both the dry and wet soil reflectance measurements. Therefore, to minimise the risk of drying the soil surface in-between scans for a wet soil, a scan time of 2s was chosen, while the contact probe light was set to medium power. The sensor was optimised and calibrated with a white Spectralon tile every 4th measurement. For each sample and level of soil moisture, three replicate scans were collected at different locations within the petri dish and then averaged. To exclude noisy ranges, the spectral interval was narrowed to 400–2500nm.

After collecting dry soil reflectance, the dry samples were weighed and water was slowly poured from a graduated cylinder, allowing precise control of the volume applied to each sample to reach ~35% gravimetric soil moisture. Care was taken while adding water to minimise disturbance of the soil surface and maintain its natural structure and roughness within the petri dish. The petri dishes were covered with lids for ~2h to allow moisture homogenisation within the soil sample. After 2h, the samples were weighed to calculate the new gravimetric soil moisture content using Equation (1):

$$Soil\ moisture\ (gravimetric) = \frac{(Ww - Wd)}{Wd} \tag{1}$$

where W_w is the weight of the wet sample and W_d is the weight of the dry sample. After determining the gravimetric soil moisture, the soil reflectance was measured for that level of soil moisture content.

The petri dishes were then placed in a vacuum pressure oven at 30°C for about an hour (consistent with a ~5% gravimetric soil moisture decrease), re-weighed to calculate the new gravimetric soil moisture content, covered with a lid for approximately 30min to ensure moisture homogenisation within the sample, weighed again to ensure no moisture loss, and finally scanned again, following the same protocol with the spectroradiometer. The samples were then placed in the vacuum oven again to dry the soil further, and the process was repeated for 30%, 25%, 20%, 15%, 10%, 5% gravimetric soil moisture contents, until the samples returned to being dry again. For samples that did not reach saturation at 35% gravimetric soil moisture, the experiment was repeated increasing the amount of water added. For a schematic summary of the re-wetting and drying process, see (Appendix A, Figure A2b). Scans acquired under visibly waterlogged conditions were discarded. The gravimetric moisture content was converted to volumetric moisture content by multiplying by each sample's bulk density, determined from soil cores collected in the field and analysed in the laboratory. Then, the reflectance at each wavelength between 400 and 2500 nm was plotted against volumetric soil moisture, and an exponential decreasing function Equation (2), Lobell and Asner (2002) was fitted through the points:

$$y = a * e^{-cx} + b \tag{2}$$

where y is the soil reflectance for a specific soil moisture content (x), a is the amplitude of reflectance change between dry and saturated soil moisture, c is the exponential rate of decay (c-factor), and b is the asymptotic minimum reflectance reached at high moisture levels. An example of curve fitting is provided in Figure 2a,b. The c-factor across each wavelength, which is an indicator of how quickly reflectance at that wavelength saturates with increasing soil moisture, was then retained and plotted for each soil sample (see Figure 2c).

The c-factor of each sample (C_o) was plotted against wavelength and normalised using L1 normalisation, a technique in which each c-factor value ($C_{o,i}$) at wavelength i is divided by the sum of all values across the wavelength range, producing a normalised c-factor value ($C_{n,i}$) (Equation 3)

$$C_{n,i} = \frac{C_{o,i}}{\sum_{i=1}^{m} C_{o,i}} \tag{3}$$

This ensures that the sum of all normalised values equals one, rescaling the data along the y-axis while preserving the relative shape of the profile. L1 normalisation allows for direct comparison of c-factor profiles across samples. For each sample, the scaling normalisation factor (n) was then obtained by dividing the original c-factor vector by the normalised vector element-wise, producing a vector of identical values across all wavelengths. The unique value from this vector was then extracted as the scalar normalisation factor n (Equation 4):

$$n = \sum_{i=1}^{m} C_{o,i} \tag{4}$$

where C_o is the original c-factor vector, and C_n is the normalised c-factor vector. Because L1 normalisation divides all elements by the same constant, this procedure produces a single scalar equal to the sum of the original c-factor values. The scalar n represents how much each profile was scaled during normalisation and was then plotted against its log-transformed soil properties (OC content, clay %, sand %, silt %, $CaCO_3$ and Ox_Fe content). Linear regression was used to investigate the relationship between each soil property and the rate at which soil reflectance decreases with increasing soil moisture. It should be noted that many samples had $CaCO_3$ values equal to zero; therefore, square root transformation was preferred to log transformation in this case. In order to better understand which soil properties influence the normalisation factor the most, the relative importance of each predictor was calculated using dominance analysis (DA) via the dominance-analysis Python package (Shekhar et al. 2019). DA fits models to all possible combinations of independent variables to then measure the goodness-of-fit (increase in R^2) associated with each variable (Azen and Budescu 2003; Budescu 1993). Due to the small sample size ($n=28$), after DA analysis, a sequential forward feature selection algorithm with a linear regression estimator and 2-fold cross-validation was used to select the ideal number of features to create a multiple linear regression model describing the behaviour of the soil moisture-reflectance relationship. The algorithm added predictors one at a time and evaluated whether each additional variable improved model performance, measured by the cross-validated R^2 score. To ensure that only variables with meaningful predictive value were retained, we applied a tolerance threshold so that a new feature was accepted only when it increased the cross-validated R^2 by more than 0.01. Once features were selected via forward feature selection, a multiple linear regression model was fitted. The model was evaluated using 4-fold cross-validation repeated 100 times. For each repetition, the rows of the dataset were randomly shuffled before splitting into folds. Out-of-fold predictions were obtained for each sample using models trained on the training folds, rather than using the model fitted on the full dataset, providing robust estimates in light of the small sample size ($n=28$). Finally, the single best-performing model was selected.

3 | Results

3.1 | Laboratory Observations

Across all 28 soil samples, the reflectance was found to decrease non-linearly with increasing soil moisture (Appendix A, Figure A3). This relationship was best represented by a decreasing exponential function in all cases (Appendix B, Table B1). The exponential rates of decay (c-factor) varied based on wavelength: as can be observed in Figure 3a, the rate of decay was higher in the visible range and decreased in the NIR and SWIR ranges. A peak at around 1900 nm was also observed. The rates of decay not only varied based on wavelength but also varied across soil samples (Figure 3a), resulting in high coefficients of variation. However, upon L1 normalisation (C_n, Equation (3)), most of the c-factor plots collapsed reasonably well onto an average line (Figure 3b), resulting in a 4-fold decrease in the coefficient of variation, reaching $<15\%$ variance from 550 to 1500 nm and from 2100 to 2300 nm (Figure 3c). Bands in the visible region (especially around 400–500 nm), wavelengths around 1900 nm and the higher SWIR bands (2300 nm onwards) did not collapse when normalisation was applied. While the C_n of some samples collapsed very well onto the average line (samples 3, 14, 22 and 26), two samples did not: sample 13, which displayed lower than average normalised c-factor values in VIS–NIR and overshoots in SWIR, around 1900 and 2400 nm; and sample 16, which displayed high L1 normalised c-factor values in VIS–NIR until around 1400 nm, before dropping to lower-than average c-factor values at higher wavelengths.

Once the normalisation factors (n, Equation (3)) were obtained for each sample and plotted against soil properties (Figure 4), it was found that OC content, clay and silt exhibited statistically significant relationships (p value <0.05) with the normalisation factor in the log–log space. In the case of OC content, a moderate decreasing relationship was observed, while for clay and silt, a moderate increasing relationship was found (see Figure 4).

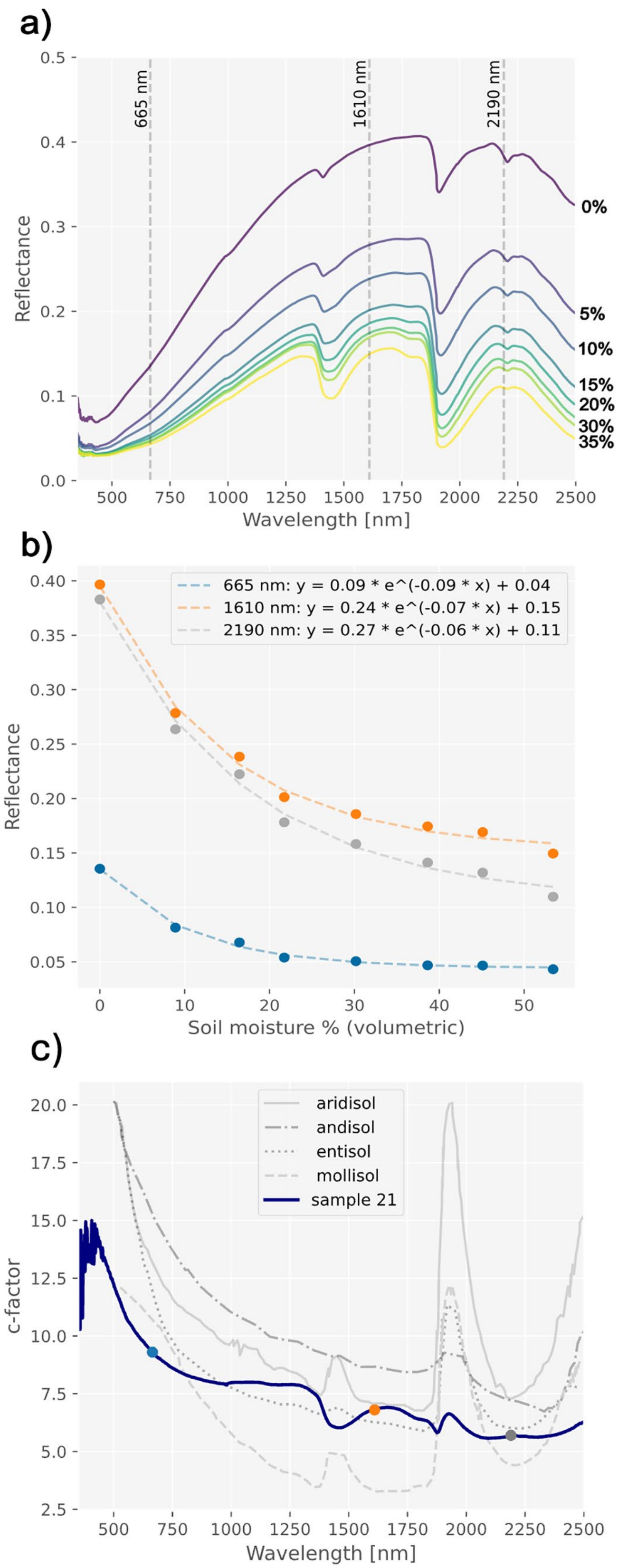

FIGURE 2 | (a) Decreasing laboratory spectral reflectance of soil sample ID 21 with increasing gravimetric soil moisture content %, which was then converted to volumetric; (b) exponential curve fitting through reflectance points at 3 wavelengths. Lower wavelengths (e.g., 665 nm) reached a reflectance plateau sooner than higher wavelengths (1610 and 2190 nm) with increasing volumetric soil moisture content; (c) building the *c*-factor plot for sample 21. The exponential factors of the curves fitted over the three wavelengths in panel 2c are highlighted using blue (665 nm), orange (1610 nm) and gray (2190 nm). *C*-factor plots of four soils analysed by Lobell and Asner (2002) are also shown.

Dominance analysis highlighted the fact that OC content explained 28% of the variance in the normalisation factor, followed by clay content (20%), silt content (10%), $CaCO_3$ (5%), sand content (4%) and finally, Ox_Fe (3%). This translates into OC, clay, and silt content having 39%, 28% and 14% relative importance, respectively. It should be noted that the DA ranking, which reflects each feature's contribution in the final model, does not necessarily match the order in which features were evaluated during forward selection. The sequential forwards feature selection algorithm selected four variables: OC content, clay, sand and silt content and discarded Ox_Fe and $CaCO_3$ content. These four variables were therefore used to fit 100 multiple linear regression models from which we obtained the cross-validated R^2 (average $R^2=0.54\pm0.09$ (SD), see Appendix D, Table D1). The equation of the single best-performing model (Equation (5), $R^2=0.67$, Figure 5) is reported below:

$$\log(n) = 8.78 - 0.47 * \log(OC) + 0.45 * \log(clay) + 0.12 * \log(silt) + 0.17 * \log(sand) \tag{5}$$

where n is the normalisation factor, OC is the organic carbon content (in $g\,kg^{-1}$), clay, sand and silt are expressed in %. The residuals of the model, defined as the differences between observed and predicted reflectance values, were approximately normally distributed. Normality was assessed using a quantile-quantile (QQ) plot (Appendix D, Figure D1). Most points fell on a straight line, supporting the assumption of normality required for valid inference in linear regression.

A visual summary of the soil moisture-relationship observed in this study is provided in Figure 6. Soil samples with coarse texture (sand and loamy sand with +80% sand content) displayed the lowest normalisation factors, regardless of their OC content. For finer textural classes, the normalisation factor seemed to vary more on OC content rather than texture (for more information, see Appendix E, Figure E1).

4 | Discussion

4.1 | Soil Reflectance Response to Increasing Moisture

The reflectance behaviour in the optical domain of 28 European soil samples of varying soil properties was investigated for different levels of volumetric soil moisture content (0% to ~60%). Soil reflectance was found to decrease non-linearly with

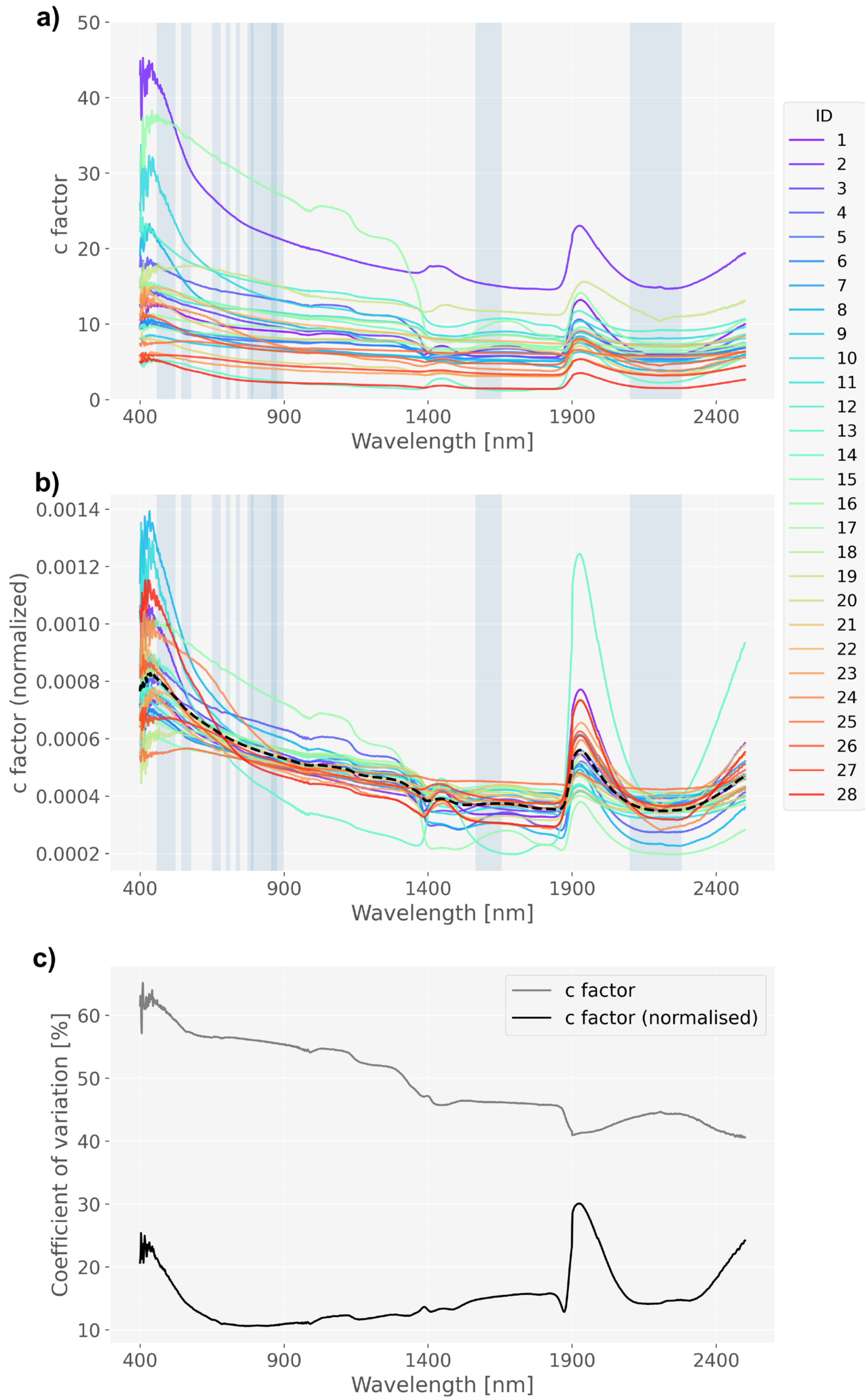

FIGURE 3 | (a) Exponential rate of decays (*c*-factors) extracted across all wavelengths for each sample; (b) normalised *c*-factors, with the average shape plotted in a dashed black line. The light blue intervals represent the spectral resolution ranges of Sentinel-2 satellite bands The average normalised *c*-factor plot is consultable in Appendix C, Figure C1; (c) coefficient of variation of the normalised and non-normalised *c*-factor plots.

increasing soil moisture content across all samples, and some samples saw an increase in reflectance under waterlogged conditions (ignored in this study), in agreement with Lobell and Asner (2002), Sadeghi et al. (2015), and Weidong et al. (2002). The rate of exponential decay (*c*-factors) varied depending on wavelength, being higher in the visible range and decreasing in the NIR and SWIR ranges, to then peak around 1900 nm, where the strongest OH absorption band is (Ben-Dor and Demattê 2015; Liu et al. 2003).

Our findings partially agree with Lobell and Asner (2002), who also used an exponential model to describe soil reflectance as

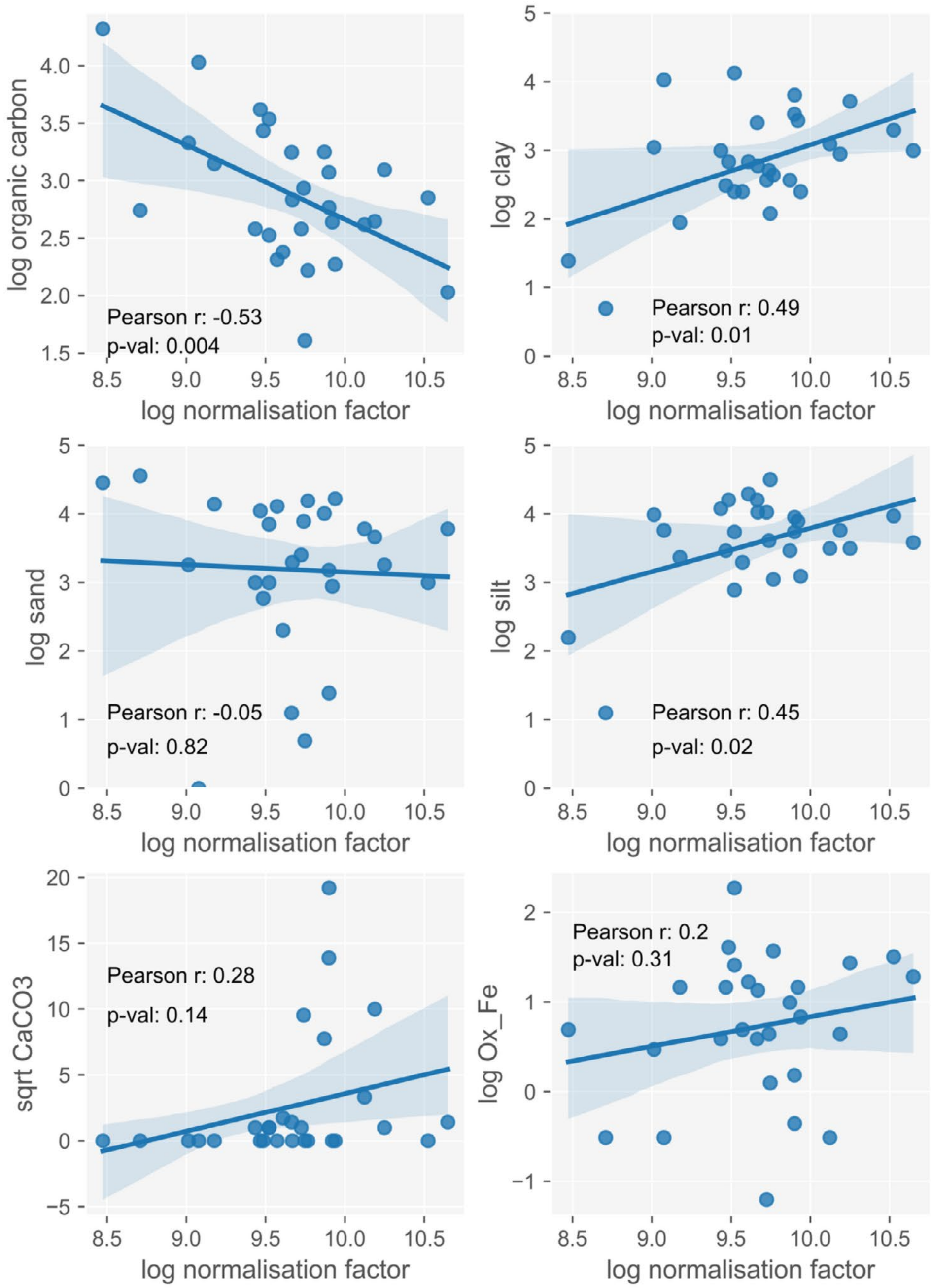

FIGURE 4 | Transformed plots of normalisation factor (*x* axis) against soil properties (*y*-axis).

a function of soil moisture, and they obtained *c*-factor plots of similar shape to the ones observed in this study. The higher the *c*-factor, the quicker the decreasing exponential function reaches a plateau, and the quicker soil reflectance lowers, reaching a saturation point as soil moisture content increases. Lobell and Asner (2002) observed that wavelengths in the visible range saturated at around 20% volumetric soil moisture content, while SWIR saturated at higher volumetric moisture contents (about 50%). The same was found in our study. This corroborates the notion that the SWIR region is better suited to monitor soil moisture content as it is affected more strongly than the visible region, which tends to saturate sooner. Other studies have also found the SWIR region to be more correlated with soil moisture content than wavelengths in the VIS–NIR (Castaldi et al. 2015). Although the *c*-factor varied significantly across soil samples, normalisation resulted in most of the *c*-factor plots collapsing onto the same line, especially between 550 and 1500 nm. Soil type-specific differences in the rates of exponential reflectance decay were also observed by Lobell and Asner (2002). However, in order to correct for these differences, they normalised the *c*-factor plots using the degree of soil saturation, a ratio of volumetric soil moisture divided by 1–(bulk density/soil particle density), where particle density was a constant set to 2.65 g cm^{-3}. We also tested the degree of saturation normalisation technique, but it didn't perform as well as L1 normalisation in making all the *c*-factor plots collapse onto the same line, probably because of the assumption of constant particle density (see Appendix F, Figures F1 and F2). Due to the variability in porosity and particle size distribution, general relationships between reflectance and soil moisture are difficult to establish (Stenberg et al. 2010). In the European soils we tested, the soil moisture-reflectance relationship was soil type-dependent and could be broadly generalised across the samples by L1 normalising them and using an average C_n. While sandy loam samples fit this generalisation well, we attribute sample 13's low c-factor values and overshoots around the water absorption bands to its extremely high sand content (95%) and moderate OC content (15.5 g kg^{-1}), which prevented the reflectance from reaching a water saturation point (see Appendix A, Figure A3). Additionally, the spectra of sample 16 with gravimetric moisture contents ≥ 10% were nearly overlapping in the 400–1000 nm range (see Appendix A, Figure A3). We suggest that the unusual behaviour may be due to the formation of a soil crust during the re-wetting and drying experiment caused by the fine texture (silt loam) and moderate clay (27%) contents of this sample. It has been theorised that crusting is more likely to form in fine-textured soils, but a ~20% clay content or lower reduces aggregate stability and hydraulic conductivity, promoting crust formation (Wakindiki and Ben-Hur 2002). Clay mineralogy has also been found to affect soil dispersity and the likelihood of crust formation, but this was not explored in this study and might constitute a reason why samples with similar textural characteristics do not deviate from the average C_n.

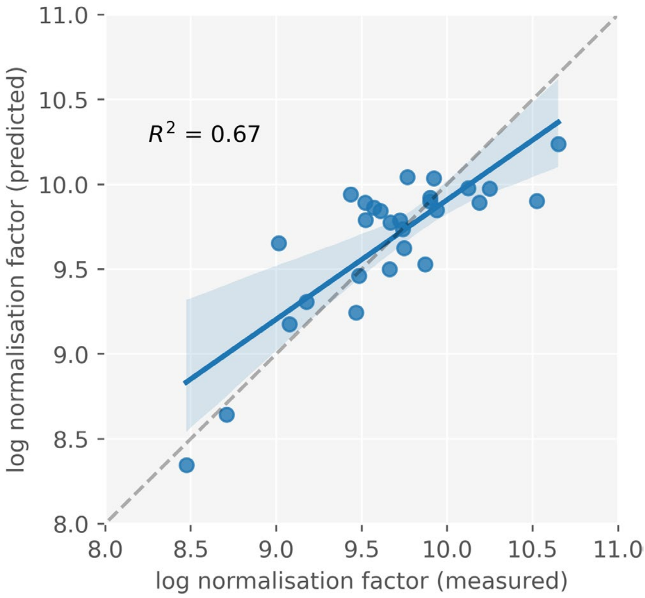

FIGURE 5 | Out-of-fold predictions (cv = 4) of the multiple linear regression model developed in this study describing the behaviour of the normalisation factor based on OC content, clay, sand and silt %. The shaded area corresponds to a 95% confidence interval.

4.2 | Influence of Soil Properties on Moisture-Reflectance Relationship

When the L1 normalisation factor of each sample was calculated and plotted against key soil properties, OC content, % clay ($p < 0.01$) and % silt ($p < 0.05$) exhibited statistically significant relationships with the normalisation factor. This supports the notion that soil properties affect the soil moisture-reflectance

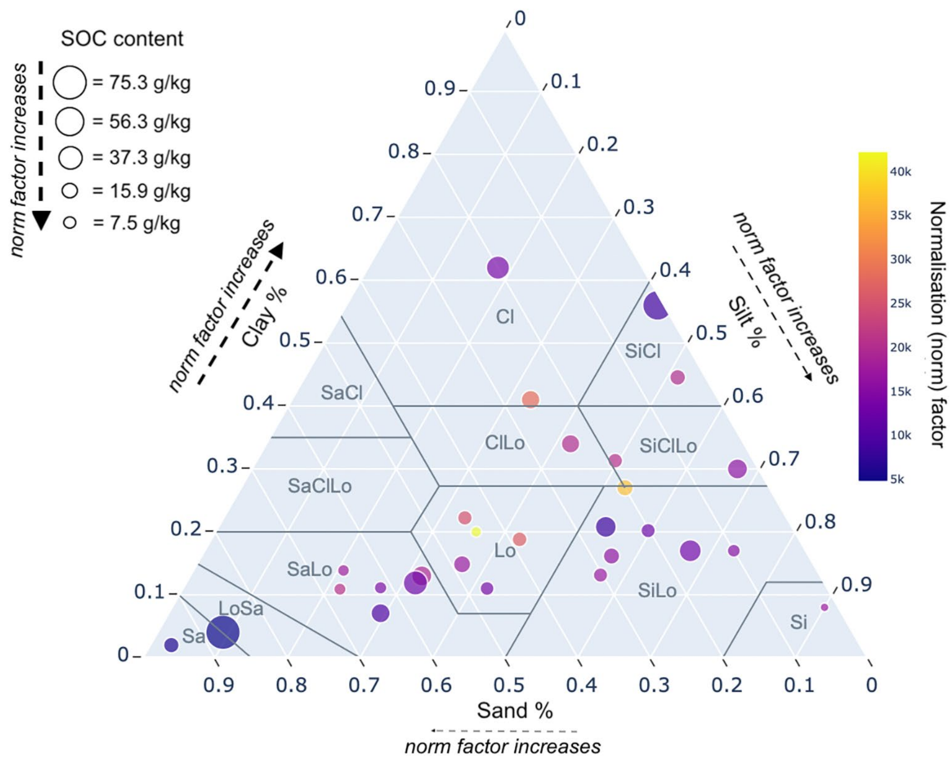

FIGURE 6 | Visual summary of how the c-factor (rate of reflectance decay with increasing soil moisture) varies based on soil properties identified in this study. The thickness of the dashed arrows represents the relative importance of each variable towards model predictions. Soil OC content and clay combined explain more than ¾ of the relative variance in normalisation factor. Cl, clay; ClLo, clay loam; Lo, loam; LoSa, loamy sand; Sa, sand; SaCl, sandy clay; SaClLo, sandy clay loam; SaLo, sandy loam; Si, silt; SiCl, silty clay; SiClLo, silty clay loam; SiLo, silty loam.

relationship (Knadel et al. 2023, 2014). When considered individually, increasing OC content was generally linked to lower normalisation factors, meaning lower rate of reflectance decay, with reflectance saturating more slowly as soil moisture content increased. This phenomenon has also been observed in an experiment on Danish soil samples by Knadel et al. (2014), where samples with higher OC content displayed a lower decrease in reflectance from wet to dry state, which was attributed to the fact that the OC content already makes the soil samples look darker, masking the spectral effect of soil moisture. A similar phenomenon was also observed by Cao et al. (2020) on soil samples of varying OC contents from inner Mongolia. It should be noted that, in addition to quantity, the type of organic carbon can also affect soil reflectance differently (Stoner and Baumgardner 1981), which is something that was not investigated in this study. When creating a model of reflectance of wetted soil (Philpot 2010) considered that the water occupying the pore space in soil often contains dissolved organic carbon which has an absorption curve that is especially dominant in the VIS range. By including the concentration of dissolved organic carbon in the equation, Philpot's model improved. In Knadel et al.'s (2014) study, the soil moisture-reflectance relationship was also found to vary based on the quantity and type of soil organic matter in sandy soils. This was attributed to the fact that organic matter in the form of humic acids, aliphatic fractions or plant debris can coat the soil particles, creating a film that makes the soil more water repellent (Chenu et al. 2000; Knadel et al. 2014).

In terms of soil texture, in our study higher clay and silt contents were associated with higher normalisation factors and subsequent higher exponential rates of decay. As moisture content increased, the reflectance decrease of clay-rich soils saturated more quickly, while the reflectance of sandy soils decreased more slowly. In Knadel et al.'s (2014) study, the reflectance of clay-rich soils, which have larger surface areas and smaller pore space but higher porosity compared to sand-rich soils, also better captured the shift from dry (characterised by water forming a thin layer around mineral particles, therefore adsorptive forces) to wet soil (characterised by the presence of free water occupying the pore space, therefore capillary forces). This is due to the refractive index between soil and air being greater than that between soil and water: when the medium around the soil particle changes from water to air, a greater contrast (in the form of higher reflectance) can be observed (Twomey et al. 1986). Nevertheless, the marked difference between wet and dry reflectance in clay-rich soils compared to sandy soils was attributed to the fact that, in sandy soils, adsorption forces are negligible and capillary forces dominate, even at lower levels of soil moisture content, therefore the drop in reflectance with increasing soil moisture is more constant (Knadel et al. 2014).

As for the combined effect of OC content and texture, we found that coarse-textured samples had lower normalisation factors (n) regardless of OC content, while in finer-textured soils, higher OC content led to a decrease in n. In a similar study, Soltani et al. (2019) found a linear relationship between soil water content and a NIR index with the intercept, which represents soil water content at saturation, varying based on the combined effect of texture and OC content. Notably, they showed that OC content generally increased the intercept, although the magnitude depended on soil texture: in coarse-textured soils, OC content substantially increased the intercept when OC levels were high due to increased sample microporosity. In fine-textured soils, the effect of OC varied based on the sand: clay ratio: in soils with a higher sand proportion, increasing OC led to higher intercept values, whereas in clay-dominated soils, the intercept was primarily determined by texture. Although Soltani et al. analysed a different spectral index, both studies highlight that the interaction between texture and OC governs soil moisture-reflectance behaviour.

4.3 | Semi-Empirical Model of Soil Reflectance-Moisture

Our DA analysis, forward feature selection and resulting multiple linear regression model indicate that OC content, clay %, silt % and sand % alone can describe the soil reflectance-moisture relationship, being able to explain up to 67% of the variance in the rate with which soil reflectance decreases with increasing soil moisture. On the other hand, Ox_Fe and $CaCO_3$ were not found to affect the soil reflectance-moisture relationship as importantly. These features were also discarded by the forward feature selection algorithm as their explanatory contribution was low: while interactions between excluded and retained variables cannot be ruled out, the feature selection process suggested that any such interactions are weak relative to the main effects of OC, clay, silt and sand.

Higher OC content was consistent with a decrease in normalisation factor, while higher clay, silt and sand content were associated with an increase in normalisation factor, meaning that soil darkens more quickly. The positive relationship between sand content and normalisation factor in the multiple linear regression model is striking, as no positive correlation was found when sand and normalisation factor were investigated individually. This might be a result of the interaction between variables in the multiple linear regression model. Despite this, OC and clay content still explained the majority of the variance.

These results highlight the importance of explicitly accounting for soil properties when investigating the soil moisture-reflectance relationship. Rodionov et al. (2014) successfully predicted soil moisture from reflectance using partial least squares regression. While their model performed very well locally ($R^2 = 0.95$), it relied on soils from a single location with similar properties, limiting its generalisability. In contrast, our semi-empirical model explicitly incorporates soil texture and OC content to generalise across a subset of European soils. Our findings suggest that physical models of soil reflectance-moisture should be adapted to simulate soil reflectance at varying levels of soil moisture on the basis of soil OC content and texture. Some physical-based models focus on simulating the soil reflectance-moisture relationship using, for instance, soil spectra transformed based on the Kubelka-Munk (KM) theory, which considers soil as an absorbing and scattering layer and assumes it to be composed of particles that are much smaller than the layer thickness (Sadeghi et al. 2015; Yuan et al. 2019). Nevertheless, the absorption and scattering coefficients, which determine how much energy is reflected by the soil, are based on soil properties (OC, texture) which are routinely not accounted for. For these reasons, soils with high porosity (clay-rich) and/or high organic matter contents tend to result in decreased model performance (Sadeghi et al. 2015; Yuan et al. 2019).

Similarly, MARMIT-2, which takes as an input three parameters related to the surface coverage fraction of water, the thickness of the water layer, and the volume fraction of soil particles, could simulate wet spectra from dry laboratory reflectance with a root mean squared error of 0.8% over a set of 225 soil samples, but with decreased performance over clay-rich soils (Dupiau et al. 2022). Dupiau et al. (2022) suggested that the performance of the model may depend more on soil properties other than texture. We found this to be true for the samples analysed in our study, as the relative importance of OC content (39%) estimated via dominance analysis was higher than the other features.

Additionally, the semi-empirical model proposed in this study could be integrated into land surface models. In the Joint UK Land Environment Simulator (JULES), bare soil albedo is spatially variable (Best et al. 2011) but is taken from a static soil map (Wilson and Henderson-Sellers 1985). Bare soil albedo can also be derived from satellite observations, which provide higher spatial resolution and dynamic information. Soil albedo decreases with humidity based on in situ observations in the Interaction between Soil, Biosphere and Atmosphere (ISBA) model (Liu et al. 2014). Similarly, in the Common Land Model (CLM), a simple linear parametrisation between soil moisture and soil colour is proposed based on parameters from the literature, disregarding soil properties (Dai et al. 2003; Kala et al. 2014).

4.4 | Study Implications

The results of this study highlight the key role of OC content and soil texture in controlling the soil moisture-reflectance relationship. By explicitly incorporating these properties, models can capture the majority of variability in reflectance responses across diverse soils, for both remote sensing and laboratory soil spectroscopy applications. The semi-empirical model developed here shows that a relatively small set of readily measurable soil properties (OC content, clay, silt, sand %) is sufficient to parameterise the soil moisture-reflectance behaviour, which could enable scaling across larger regions or integration with land surface models. In practice, for a soil sample of known properties, its reflectance response to increasing moisture can be predicted without requiring direct measurement of dry soil reflectance, which is often difficult to obtain in field conditions (see Appendix C). Furthermore, integrating soil-specific parameters into land surface models like JULES, CLM, or ISBA can enhance representations of bare soil albedo and its response to moisture and reduce biases in moisture retrievals and energy balance simulations. These models typically already include parameters related to soil albedo, soil moisture, or surface properties, and our approach allows them to explicitly account for soil OC and texture, improving predictive performance without requiring additional complex inputs. Lastly, the inclusion of these soil properties in physical soil moisture-reflectance models like KM or MARMIT-2 could reduce uncertainties associated with modelling reflectance at varying levels of soil moisture, especially over clay-rich soils. Overall, our results emphasise that explicitly considering soil properties like OC content and texture is essential for accurately modelling and interpreting soil reflectance under varying moisture conditions, with potential benefits for field spectroscopy, remote sensing and land surface modelling applications.

4.5 | Limitations and Future Directions

A key limitation of this study is the restricted sample size ($n = 28$) and diversity of the dataset, which was constrained by the labour-intensive nature of the rewetting procedure. Even though the sample set was selected to cover a wide range of soil properties being investigated (OC content, texture, $CaCO_3$ and Ox_Fe), the dataset does not encompass the full pedological variability of European cropland soils: Luvisols and Cambisols (which represent ~55% of LUCAS 2018 cropland points surveyed) dominate the sample set, and several soil types are underrepresented or missing (e.g., Podzols, Regosols, Planosols, Calcisols). The distribution of soil hues also shows limited representation of bright, carbonate-rich soils and strongly iron-oxide-influenced soils, which may affect reflectance-moisture behaviour, particularly in the visible and SWIR regions. Additionally, different spectra acquisition and rewetting protocols might lead to different results. Rodionov et al. (2014) highlighted that an issue with spectroscopy is that gravimetric soil moisture might not necessarily reflect what the sensor detects due to the limited penetration depth. We tried to overcome this by covering the samples with lids before scanning to ensure moisture was more homogeneous throughout the soil column.

Consequently, while the results highlight robust trends driven primarily by texture and organic carbon, and our cross-validated feature selection and careful model construction indicate that the main effects are robust, the limited sample size should be considered when interpreting the generalisability of these results, and future work should incorporate a larger and more diverse set of soils to strengthen model calibration and assess its generalisability across the full range of European soil environments. Further studies are also needed regarding the effect of the type of organic matter on soil reflectance at various levels of soil moisture. In addition, the model's usefulness in a field spectroscopy or satellite remote sensing context still needs to be assessed. This will be particularly challenging as satellite data will suffer from higher signal-to-noise ratio and additional noise at the water absorption wavelengths due to the atmospheric effects (Knadel et al. 2023). Furthermore, the model requires a priori soil property data, which might not always be readily available especially in a remote sensing context. However, it should be noted that information on OC, clay, sand and silt content could also be obtained from digital soil mapping products, such as the LUCAS-derived topsoil property maps (Ballabio et al. 2016) or the ISRIC SoilGrids (Poggio et al. 2021). As for the soil moisture information, new maps of surface soil moisture in the topmost 0–5 cm of soil are being developed, such as the Global Surface Soil Moisture 1 km dataset (Han et al. 2023) or the SMAP Level-4 data (Reichle et al. 2019). Nevertheless, these types of data are subject to uncertainties.

5 | Conclusion

This study investigated the laboratory soil moisture-reflectance relationship for 28 European soil samples representing a range of soil properties (OC content, texture, $CaCO_3$ and Ox_Fe content). Upon rewetting the soil samples and acquiring their spectral reflectance in the laboratory, soil reflectance decreased exponentially with increasing soil moisture, with faster rates of decay across visible wavelengths and slower in SWIR, and displaying varying rates across samples. Certain soil properties significantly influenced the rate of decay: higher OC content led to a slower decrease in reflectance with increasing soil moisture. At the same time, higher contents of clay and silt led to a quicker saturation of reflectance with increasing soil moisture, likely due to increased porosity and a more evident switch from water adsorption to capillarity. The multiple linear regression model created here to describe the rate of reflectance decay with increasing soil moisture based on selected soil properties (organic carbon content, clay, sand and silt content) was able to explain up to 67% of the variance and could potentially be used to back-calculate dry soil reflectance from timeseries of wet reflectance. Future work should test this model on additional soil samples (different geographical regions, soil types and colours), and on field-acquired or remotely-sensed spectra. Finally, the semi-empirical model proposed here could be incorporated into land surface models to overcome the underexplored connection between soil moisture content and bare soil albedo.

Author Contributions

D. Hick: conceptualization, methodology, data curation, software, formal analysis, visualization, writing – original draft. **P. J. Chapman:** supervision, methodology, writing – review and editing. **T. S. Breure:** methodology, writing – review and editing, resources. **G. Ziv:** conceptualization, methodology, supervision, writing – review and editing.

Acknowledgements

The LUCAS 2018 topsoil samples used in this work were kindly provided by the European Commission through the European Soil Data Centre managed by the Joint Research Centre (JRC), http://esdac.jrc.ec.europa.eu. We thank Timo Breure and Arwyn Jones (JRC), as well as Robbie Ramsay (FSF) and the University of Leeds Geography Laboratory staff for their support.

Funding

This research has been supported by the Natural Environment Research Council (NERC) through a SENSE CDT studentship (NE/T00939X/1) and the NERC Field Spectroscopy Facility via equipment loan (934.1506).

Conflicts of Interest

The authors declare no conflicts of interest.

Data Availability Statement

The datasets and code used to reproduce the figures and analyses in this study are publicly available on Zenodo: https://doi.org/10.5281/zenodo.19462976.

References

Allen, S. E., H. M. Grimshaw, J. A. Parkinson, and C. Quarmby. 1974. *Chemical Analysis of Ecological Materials*. Blackwell Scientific Publications.

Ångström, A. 1925. "The Albedo of Various Surfaces of Ground." *Geografiska Annaler* 7: 323–342. https://doi.org/10.1080/20014422.1925.11881121.

Azen, R., and D. V. Budescu. 2003. "The Dominance Analysis Approach for Comparing Predictors in Multiple Regression." *Psychological Methods* 8: 129–148.

Bablet, A., P. V. H. Vu, S. Jacquemoud, et al. 2018. "MARMIT: A Multilayer Radiative Transfer Model of Soil Reflectance to Estimate Surface Soil Moisture Content in the Solar Domain (400–2500 Nm)." *Remote Sensing of Environment* 217: 1–17.

Ballabio, C., P. Panagos, and L. Monatanarella. 2016. "Mapping Topsoil Physical Properties at European Scale Using the LUCAS Database." *Geoderma* 261: 110–123.

Baumgardner, M. F., L. F. Silva, L. L. Biehl, and E. R. Stoner. 1986. "Reflectance Properties of Soils." *Advances in Agronomy* 38: 1–44.

Ben-Dor, E. 2002. "Quantitative Remote Sensing of Soil Properties." In *Quantitative Remote Sensing of Soil Properties*. Elsevier.

Ben-Dor, E., and J. A. Demattê. 2015. "Remote Sensing of Soil in the Optical Domains." In *Land Resources Monitoring, Modeling, and Mapping With Remote Sensing*, 733–788. CRC Press.

Best, M. J., M. Pryor, D. B. Clark, et al. 2011. "The Joint UK Land Environment Simulator (JULES), Model Description–Part 1: Energy and Water Fluxes." *Geoscientific Model Development* 4: 677–699.

Blakemore, L. C., P. L. Searle, and B. K. Daly. 1987. *Methods for Chemical Analysis of Soils*. New Zealand Soil Bureau Scientific.

Budescu, D. V. 1993. "Dominance Analysis: A New Approach to the Problem of Relative Importance of Predictors in Multiple Regression." *Psychological Bulletin* 114: 542–551.

Cao, Y., N. Bao, S. Liu, W. Zhao, and S. Li. 2020. "Reducing Moisture Effects on Soil Organic Carbon Content Prediction in Visible and Near-Infrared Spectra With an External Parameter Othogonalization Algorithm." *Canadian Journal of Soil Science* 100: 253–262. https://doi.org/10.1139/cjss-2020-0009.

Castaldi, F., A. Palombo, S. Pascucci, S. Pignatti, F. Santini, and R. Casa. 2015. "Reducing the Influence of Soil Moisture on the Estimation of Clay From Hyperspectral Data: A Case Study Using Simulated PRISMA Data." *Remote Sensing* 7: 15561–15582.

Chenu, C., Y. Le Bissonnais, and D. Arrouays. 2000. "Organic Matter Influence on Clay Wettability and Soil Aggregate Stability." *Soil Science Society of America Journal* 64: 1479–1486. https://doi.org/10.2136/sssaj2000.6441479x.

Dai, Y., X. Zeng, R. E. Dickinson, et al. 2003. "The Common Land Model." *Bulletin of the American Meteorological Society* 84: 1013–1024.

Dupiau, A., S. Jacquemoud, X. Briottet, et al. 2022. "MARMIT-2: An Improved Version of the MARMIT Model to Predict Soil Reflectance as a Function of Surface Water Content in the Solar Domain." *Remote Sensing of Environment* 272: 112951.

EEA. 2016. "Biogeographical Regions, Europe 2016 (DAT-85-En)." Available Online at. https://sdi.eea.europa.eu/catalogue/idp/api/records/c6d27566-e699-4d58-a132-. bbe3fe01491b [Accessed 9 June 2025].

Fernandez-Ugalde, O., S. Scarpa, A. Orgiazzi, et al. 2022. "LUCAS 2018 Soil Module. Present. Dataset Results EUR 31144."

Grafström, A., and J. Lisic. 2018. "BalancedSampling: Balanced and Spatially Balanced Sampling. R Package Version 1.5.4." Available online. http://www.antongrafstrom.se/balancedsampling. [Accessed 9 June 2025].

Han, Q., Y. Zeng, L. Zhang, et al. 2023. "Global Long Term Daily 1 Km Surface Soil Moisture Dataset With Physics Informed Machine Learning." *Scientific Data* 10: 101.

Haubrock, S.-N., S. Chabrillat, C. Lemmnitz, and H. Kaufmann. 2008. "Surface Soil Moisture Quantification Models From Reflectance Data

Under Field Conditions." *International Journal of Remote Sensing* 29: 3–29. https://doi.org/10.1080/01431160701294695.

He, T., F. Gao, S. Liang, and Y. Peng. 2019. "Mapping Climatological Bare Soil Albedos Over the Contiguous United States Using MODIS Data." *Remote Sensing* 11: 666.

Jones, A., O. Fernandez-Ugalde, and S. Scarpa. 2020. "LUCAS 2015 Topsoil Survey. Presentation of Dataset and Results, EUR 30332 EN, Publications Office of the European Union: Luxembourg. JRC121325 DOI 10, 616084."

Kala, J., J. P. Evans, A. J. Pitman, et al. 2014. "Implementation of a Soil Albedo Scheme in the CABLEv1. 4b Land Surface Model and Evaluation Against MODIS Estimates Over Australia." *Geoscientific Model Development* 7: 2121–2140.

Knadel, M., F. Castaldi, R. Barbetti, E. Ben-Dor, A. Gholizadeh, and R. Lorenzetti. 2023. "Mathematical Techniques to Remove Moisture Effects From Visible–Near-Infrared–Shortwave-Infrared Soil Spectra—Review." *Applied Spectroscopy Reviews* 58: 629–662. https://doi.org/10.1080/05704928.2022.2128365.

Knadel, M., F. Deng, A. Alinejadian, L. Wollesen De Jonge, P. Moldrup, and M. H. Greve. 2014. "The Effects of Moisture Conditions-From Wet to Hyper Dry-On Visible Near-Infrared Spectra of Danish Reference Soils." *Soil Science Society of America Journal* 78: 422–433. https://doi.org/10.2136/sssaj2012.0401.

Li, Z.-L., P. Leng, C. Zhou, K.-S. Chen, F.-C. Zhou, and G.-F. Shang. 2021. "Soil Moisture Retrieval From Remote Sensing Measurements: Current Knowledge and Directions for the Future." *Earth Science Reviews* 218: 103673. https://doi.org/10.1016/j.earscirev.2021.103673.

Liu, S., J.-L. Roujean, A. T. K. Tchuente, X. Ceamanos, and J.-C. Calvet. 2014. "A Parameterization of SEVIRI and MODIS Daily Surface Albedo With Soil Moisture: Calibration and Validation Over Southwestern France." *Remote Sensing of Environment* 144: 137–151.

Liu, W., F. Baret, X. Gu, B. Zhang, Q. Tong, and L. Zheng. 2003. "Evaluation of Methods for Soil Surface Moisture Estimation From Reflectance Data." *International Journal of Remote Sensing* 24: 2069–2083. https://doi.org/10.1080/01431160210163155.

Lobell, D. B., and G. P. Asner. 2002. "Moisture Effects on Soil Reflectance." *Soil Science Society of America Journal* 66: 722–727. https://doi.org/10.2136/sssaj2002.7220.

McGuirk, S. L., and I. H. Cairns. 2024. "Relationships Between Soil Moisture and Visible–NIR Soil Reflectance: A Review Presenting New Analyses and Data to Fill the Gaps." *Geotechnics* 4: 78–108.

Minasny, B., A. B. McBratney, V. Bellon-Maurel, et al. 2011. "Removing the Effect of Soil Moisture From NIR Diffuse Reflectance Spectra for the Prediction of Soil Organic Carbon." *Geoderma* 167: 118–124.

Muller, E., and H. Decamps. 2001. "Modeling Soil Moisture–Reflectance." *Remote Sensing of Environment* 76: 173–180.

Nocita, M., A. Stevens, B. van Wesemael, et al. 2015. "Soil Spectroscopy: An Alternative to Wet Chemistry for Soil Monitoring." *Advances in Agronomy* 132: 139–159.

Philpot, W. 2010. "Spectral Reflectance of Wetted Soils." *Proceedings of ASD and IEEE GRS* 2: 1–12.

Poggio, L., L. M. De Sousa, N. H. Batjes, et al. 2021. "SoilGrids 2.0: Producing Soil Information for the Globe With Quantified Spatial Uncertainty." *Soil* 7: 217–240.

Reichle, R. H., Q. Liu, R. D. Koster, et al. 2019. "Version 4 of the SMAP Level-4 Soil Moisture Algorithm and Data Product." *Journal of Advances in Modeling Earth Systems* 11: 3106–3130. https://doi.org/10.1029/2019MS001729.

Rodionov, A., S. Pätzold, G. Welp, R. C. Pallares, L. Damerow, and W. Amelung. 2014. "Sensing of Soil Organic Carbon Using Visible and Near-Infrared Spectroscopy at Variable Moisture and Surface Roughness." *Soil Science Society of America Journal* 78, no. 3: 949–957.

Roger, J.-M., F. Chauchard, and V. Bellon-Maurel. 2003. "EPO–PLS External Parameter Orthogonalisation of PLS Application to Temperature-Independent Measurement of Sugar Content of Intact Fruits." *Chemometrics and Intelligent Laboratory Systems* 66: 191–204.

Sadeghi, M., S. B. Jones, and W. D. Philpot. 2015. "A Linear Physically-Based Model for Remote Sensing of Soil Moisture Using Short Wave Infrared Bands." *Remote Sensing of Environment* 164: 66–76. https://doi.org/10.1016/j.rse.2015.04.007.

Sanderman, J., C. Partida, J. L. Safanelli, et al. 2025. "Application of a Handheld Near Infrared Spectrophotometer to Farm-Scale Soil Carbon Monitoring." *European Journal of Soil Science* 76: e70053. https://doi.org/10.1111/ejss.70053.

Shekhar, S., S. Bhagat, K. Sivakumar, and B. Koteshwar. 2019. "The Dominance Analysis Package." Available Online at. https://dominance-analysis.github.io/dominance-analysis/. [Accessed 17 June 2025].

Soltani, I., Y. Fouad, D. Michot, P. Bréger, R. Dubois, and C. Cudennec. 2019. "A Near Infrared Index to Assess Effects of Soil Texture and Organic Carbon Content on Soil Water Content." *European Journal of Soil Science* 70, no. 1: 151–161.

Stenberg, B., R. A. V. Rossel, A. M. Mouazen, and J. Wetterlind. 2010. "Visible and Near Infrared Spectroscopy in Soil Science." *Advances in Agronomy* 107: 163–215.

Stoner, E. R., and M. F. Baumgardner. 1981. "Characteristic Variations in Reflectance of Surface Soils." *Soil Science Society of America Journal* 45: 1161–1165. https://doi.org/10.2136/sssaj1981.03615995004500060031x.

Tian, J., and W. D. Philpot. 2015. "Relationship Between Surface Soil Water Content, Evaporation Rate, and Water Absorption Band Depths in SWIR Reflectance Spectra." *Remote Sensing of Environment* 169: 280–289.

Twomey, S. A., C. F. Bohren, and J. L. Mergenthaler. 1986. "Reflectance and Albedo Differences Between Wet and Dry Surfaces." *Applied Optics* 25: 431–437.

van Reeuwijk, L. P. 1995. "Procedures for Soil Analysis."

Viscarra Rossel, R. A., T. Behrens, E. Ben-Dor, et al. 2022. "Diffuse Reflectance Spectroscopy for Estimating Soil Properties: A Technology for the 21st Century." *European Journal of Soil Science* 73: e13271. https://doi.org/10.1111/ejss.13271.

Wakindiki, I. I. C., and M. Ben-Hur. 2002. "Soil Mineralogy and Texture Effects on Crust Micromorphology, Infiltration, and Erosion." *Soil Science Society of America Journal* 66: 897–905. https://doi.org/10.2136/sssaj2002.8970.

Weidong, L., F. Baret, G. Xingfa, T. Qingxi, Z. Lanfen, and Z. Bing. 2002. "Relating Soil Surface Moisture to Reflectance." *Remote Sensing of Environment* 81: 238–246.

Wilson, M. F., and A. Henderson-Sellers. 1985. "A Global Archive of Land Cover and Soils Data for Use in General Circulation Climate Models." *Journal of Climatology* 5: 119–143. https://doi.org/10.1002/joc.3370050202.

Yuan, J., X. Wang, C. Yan, S. Wang, X. Ju, and Y. Li. 2019. "Soil Moisture Retrieval Model for Remote Sensing Using Reflected Hyperspectral Information." *Remote Sensing* 11: 366.

Appendix A

Soil Samples, Methodology Illustrations and Soil Spectra

FIGURE A1 | The soil samples used in this study had various textures, hues and colours. To determine the amount of soil placed in each 90-mm petri dish, we first calculated the volume of a 0.7-cm thick soil layer (44.53 cm^3). For each sample, the target mass was obtained by multiplying this volume by the field-measured bulk density. This typically resulted in a mass close to ~50 g. Minor adjustments were made by lightly packing the soil in the dish to reproduce the target bulk density as closely as possible.

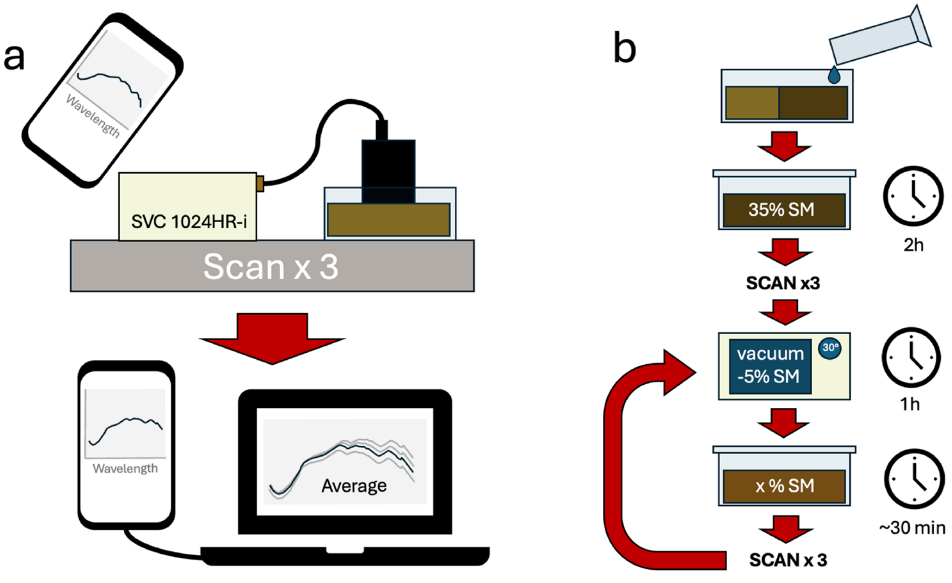

FIGURE A2 | (a) Illustration of spectra collection procedure; (b) flowchart illustrating the rewetting and drying procedure carried out in this study.

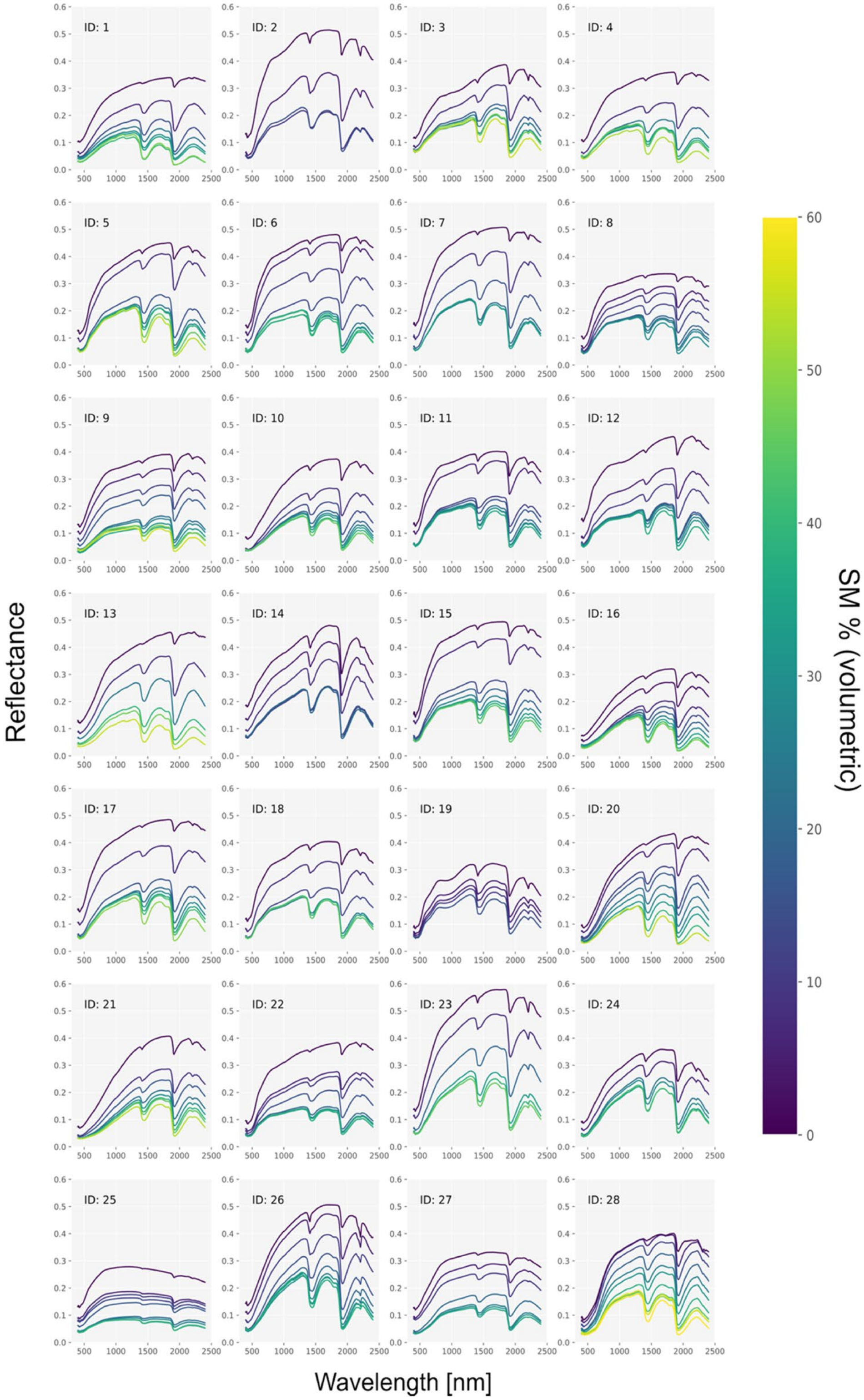

FIGURE A3 | Reflectance of soil samples analysed in this study with increasing volumetric soil moisture content. In the case of sample IDs 2 and 19, measurements were stopped at 15% as beyond that soil moisture content, the sample completely saturated with water. In some samples (IDs 1, 3, 9, 28), reflectance slightly increased at high moisture (saturation) conditions, especially at wavelengths < 1400 nm, due to a change in scattering processes caused by a water film. Scans where this phenomenon was observed were removed.

Appendix B

Fitting the Exponential Function

TABLE B1 | Goodness of fit of exponential curve to the reflectance-soil moisture data measured in this study, averaged across all wavelengths.

Sample ID	Goodness of fit ($R^2 \pm$ SD)
1	0.989 ± 0.008
2	0.990 ± 0.005
3	0.991 ± 0.005
4	0.985 ± 0.004
5	0.983 ± 0.009
6	0.934 ± 0.015
7	0.965 ± 0.011
8	0.946 ± 0.014
9	0.988 ± 0.005
10	0.997 ± 0.001
11	0.951 ± 0.163
12	0.992 ± 0.002
13	0.992 ± 0.004
14	0.972 ± 0.007
15	0.962 ± 0.008
16	0.979 ± 0.014
17	0.985 ± 0.005
18	0.965 ± 0.013
19	0.993 ± 0.005
20	0.989 ± 0.004
21	0.995 ± 0.002
22	0.988 ± 0.005
23	0.995 ± 0.004
24	0.990 ± 0.006
25	0.962 ± 0.005
26	0.966 ± 0.013
27	0.972 ± 0.008
28	0.969 ± 0.013

Appendix C

Average *c*-Factor Plot

For a given soil sample of known OC content and soil texture, for which various soil spectra are obtained at known levels of soil moisture content, the normalisation factor, a proxy for how quickly soil reflectance decreases with increasing soil moisture content, can be calculated using the semi-empirical equation derived in this study. The result can then be multiplied by the average *c*-factor line obtained in this study (Figure C1) in order to obtain the predicted soil reflectance-moisture behaviour for the soil type at hand. An exponential curve with a rate of decay equal to the *c*-factor obtained could then be made to fit through the points, and the soil reflectance at zero soil moisture content could potentially be back-calculated if dry soil reflectance data is not available (e.g., in the field).

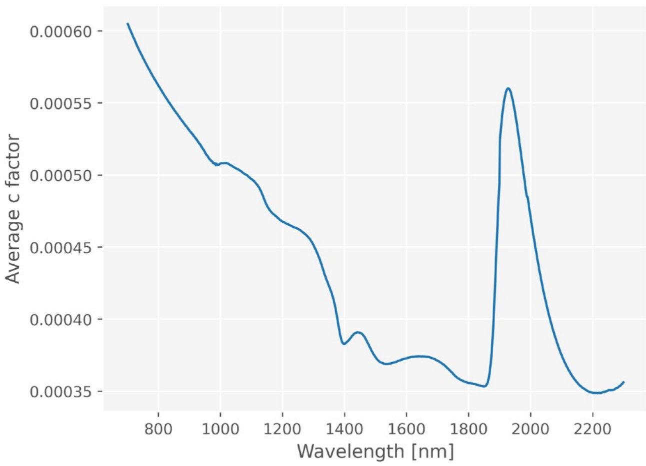

FIGURE C1 | Average *c*-factor plot obtained in this study across the 28 soil samples investigated. Future studies could use the equation provided to calculate the normalisation factor for the soil type at hand, then multiply it by the line shown in the picture to obtain the *c*-factor for that sample across all wavelengths. This will indicate how quickly the reflectance decreases with increasing soil moisture content across different wavelengths for that soil type.

Appendix D

Normalisation Factor Predictions

TABLE D1 | Variance of coefficients for the semi-empirical model to predict the normalisation factor based on soil properties across the 100 model runs.

Variables	Mean ± SD
Intercept	$8.78 \pm 8.93 \times 10^{-15}$
Coefficient for OC	$-0.47 \pm 7.81 \times 10^{-16}$
Coefficient for clay	$0.45 \pm 6.69 \times 10^{-16}$
Coefficient for silt	$0.12 \pm 2.65 \times 10^{-16}$
Coefficient for sand	$0.17 \pm 3.07 \times 10^{-16}$

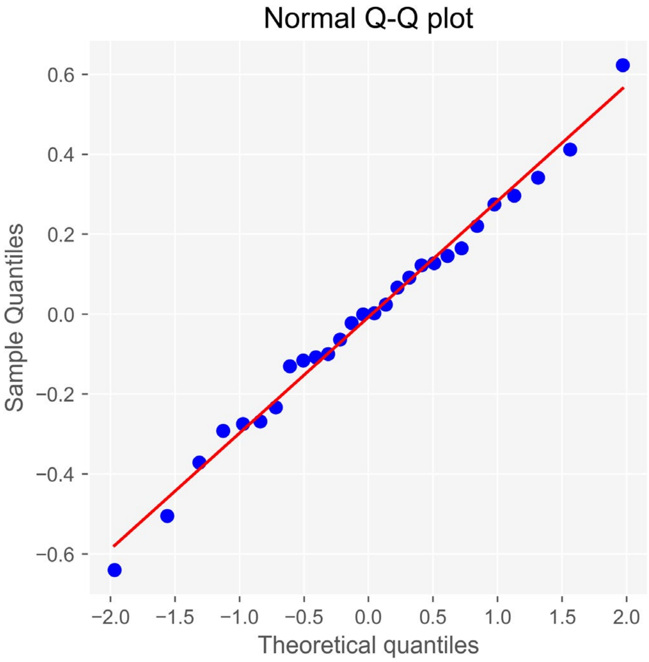

FIGURE D1 | Quantile-quantile plot of residuals (observed—out-of-fold predicted values) of the single best-performing model to predict normalisation factor based on OC content and soil texture.

Appendix E

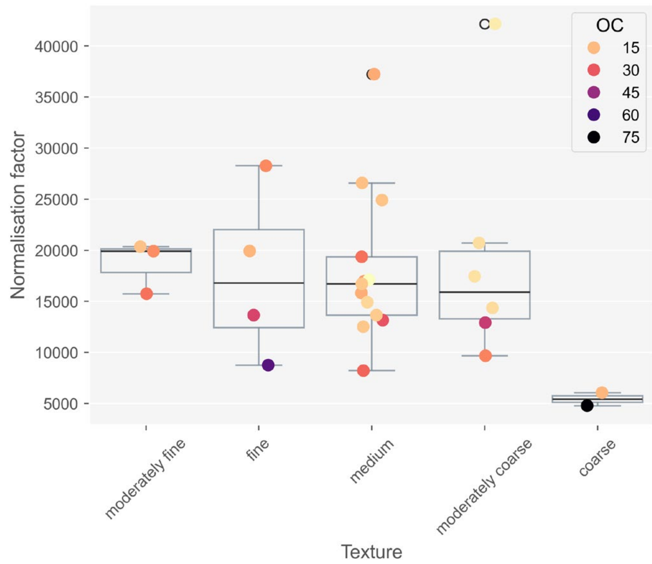

FIGURE E1 | Spread of normalisation factors by soil texture group. Coarse = sand, loamy sand; moderately coarse = sandy loam; medium = loam, silty loam, silt; moderately fine = clay loam, sandy clay loam, silty clay loam; fine = clay, sandy clay, silty clay.

Appendix F

Comparing *c*-Factor Normalisation Methods

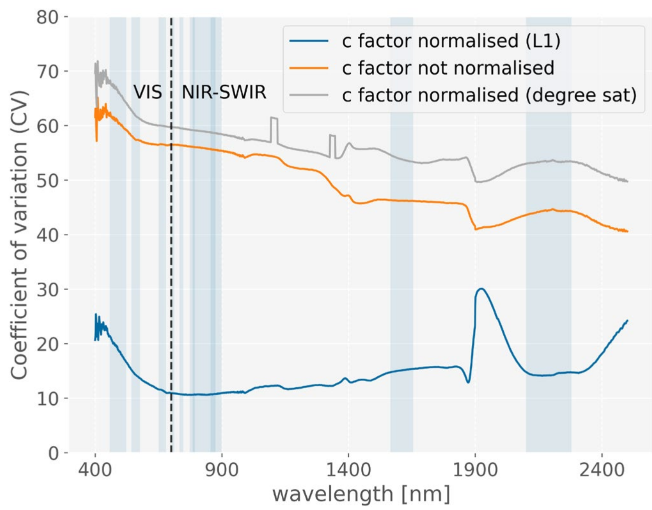

FIGURE F1 | Coefficient of variation plots of the *c*-factors lines obtained in this study. While degree of saturation normalisation led to higher coefficient of variation, probably due to the assumption of standard particle density, L1 normalisation led to a decrease in the coefficient of variation. Regions where the normalised *c*-factor plots did not collapse as well were below 450 nm, between 1900 and 2000 nm (water absorption peak) and beyond 2300 nm.

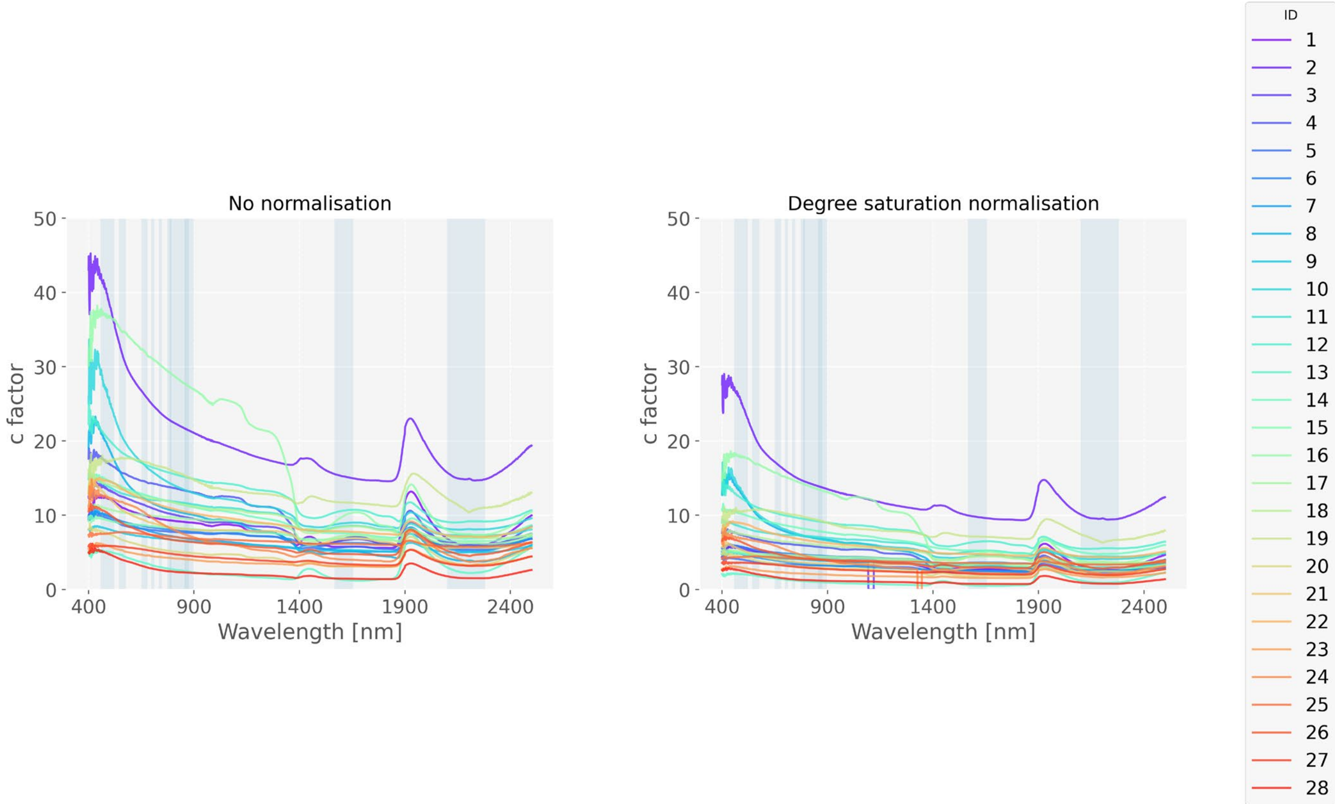

FIGURE F2 | *C*-factor (left) and normalised *c*-factor (right) according to the Lobell and Asner's (2002) degree of saturation normalisation method.